The Canadian Mineralogist
Vol. 37, pp. 37-52 (1999)

As, Sb, Be AND Ce ENRICHMENT IN MINERALS FROM A METAMORPHOSED Fe–Mn DEPOSIT, VAL FERRERA, EASTERN SWISS ALPS

JOËL BRUGGER[1]

Mineralogisch-Petrographisches Institut der Universität, Bernoullistrasse 30, CH-4056 Basel, Switzerland

RETO GIERÉ

Department of Earth and Atmospheric Sciences, Purdue University, West Lafayette, Indiana 47907-1397, U.S.A.

Abstract

Several small syngenetic-exhalative Fe–Mn deposits metamorphosed under blueschist- to greenschist-facies conditions occur in Triassic marbles of the Middle Penninic nappes in Val Ferrera (eastern Swiss Alps). Pink muscovite – aegirine – hematite – albite schists associated with the ores in one of these deposits (Starlera mine) contain an unusual assemblage of As-, Sb-, Be-, and *REE*-rich minerals that developed after the main deformation (D_1). In these pink schists, As is present in significant amounts in both titanite (to 3.46 wt% As_2O_5) and fluorapatite (to 13.8 wt% As_2O_5), and is a major component of bergslagite, $CaBeAsO_4(OH)$. Antimony is an essential constituent of rutile (to 30.63 wt% Sb_2O_5), titanite (to 9.55 wt% Sb_2O_5), and pyrophanite (to 1.91 wt% Sb_2O_5), in which it is accommodated *via* the exchange vector $Sb^{5+}Fe^{3+}Ti^{4+}_{-2}$. Roméite, $(Ca,Na,\square)_2(Sb,Ti)_2O_6(F,OH,O)$, is also an important host for Sb, but in addition it incorporates major amounts of *REE* (to 23.4 wt% Ce_2O_3). The pink schists at Starlera are the second reported occurrence of natural Sb-rich rutile and Sb-rich titanite (after Praborna, western Italian Alps), and the third of As-bearing titanite (Praborna and Wannigletscher, Binntal, central Swiss Alps). The Starlera deposit is further characterized by the presence of thick veins of roméite–tilasite ($CaMgAsO_4F$). Most of these late (post-D_1) veins are closely associated with intensely foliated pink schists, indicating that they formed from fluids that passed through the schists. These fluids must have carried As, Sb, and Ti, and probably were similar to those responsible for growth of the post-D_1 As, Sb, Be, Ti, and *REE* minerals in the pink schists. The metal content of the fluids was most likely derived from the surrounding ores. The unusual assemblages in both veins and pink schists at Starlera document mobility of As, Sb, Be, Ti, and *REE* under lower greenschist-facies conditions and in a relatively oxidizing environment.

Keywords: Fe–Mn deposit, rutile, titanite, roméite, fluorapatite, bergslagite, Val Ferrera, Swiss Alps.

Sommaire

Les marbres triassiques des nappes du Pennique Moyen renferment dans le Val Ferrera (Alpes suisses orientales) plusieurs petits gîtes syngénétiques exhalatifs métamorphisés aux conditions des faciès schistes verts à schistes bleus. Des schistes roses à muscovite – aegyrine – hématite – albite associés aux minerais d'un de ces gisements (mine de Starlera) contiennent un assemblage inhabituel de minéraux enrichis en As, Sb, Be, et terres rares (TR). Cet assemblage s'est développé après la déformation principale (D_1). Dans ces schistes roses, l'As est présent dans la titanite (jusqu'à 3.46% poids As_2O_5) et la fluorapatite (jusqu'à 13.8% poids As_2O_5), et est un composant essentiel de la bergslagite, $CaBeAsO_4(OH)$. L'antimoine est enrichi dans le rutile (jusqu'à 30.63 % poids Sb_2O_5), la titanite (jusqu'à 9.55 % poids Sb_2O_5), et la pyrophanite (jusqu'à 1.91 % poids Sb_2O_5). Le Sb est incorporé dans ces minéraux selon le vecteur d'échange $Sb^{5+}Fe^{3+}Ti^{4+}_{-2}$. La roméite, $(Ca,Na,\square)_2(Sb,Ti)_2O_6(F,OH,O)$, est aussi un important hôte de Sb, et incorpore en outre de grandes quantités de TR (jusqu'à 23.4 % poids Ce_2O_3). Les schistes roses de Starlera sont, après Praborna (Alpes italiennes occidentales), le second indice de rutile et de titanite riches en Sb, et le troisième indice de titanite arsenicale après Starlera et Wannigletscher (Binntal, Alpes suisses centrales). Le gîte contient aussi d'épaisses veines de roméite et tilasite ($CaMgAsO_4F$). La plupart de ces veines tardives (post-D_1) sont associées intimement à ces schistes roses, ce qui fait penser qu'elles se sont formées à partir de fluides circulant dans les schistes. Ces fluides doivent avoir transporté As, Sb, et Ti, et étaient probablement identiques à ceux responsables de la croissance post-D_1 de minéraux à As, Sb, Be, Ti et TR dans les schistes roses. Les métaux ainsi mobilisés proviendraient vraisemblablement des minerais encaissants. La minéralogie inhabituelle des veines et des schistes roses de Starlera documente la mobilité de As, Sb, Be, Ti et TR sous conditions du faciès schistes verts inférieur en milieu relativement oxydant.

Mots-clés: gisement Fe–Mn, rutile, titanite, roméite, fluorapatite, bergslagite, Val Ferrera, Alpes suisses.

[1] *Present address*: Department of Earth Sciences, Monash University, Clayton, Victoria 3168, Australia. *E-mail address*: joelb@earth.monash.edu.au

Introduction

The metamorphism of Mn ores commonly produces complex mineral associations of silicates, oxides, and carbonates (*e.g.*, Roy 1968, Chopin 1978, Peters *et al.* 1980, Abrecht 1989, Dasgupta *et al.* 1989). Some metamorphosed Mn deposits are also known for their amazing diversity of accessory minerals, containing elements such as As, Sb, and Be; most famous among these deposits are Långban, Sweden (Boström *et al.* 1979, Holtstam *et al.* 1998), which is the type locality of 68 new species (Aleph Computer/CSIRO mineral database 1995), Franklin, New Jersey (Dunn 1995; 50 new species), and the Kombat mine in Namibia (Dunn 1991; seven new species).

In the Alps, many small Mn deposits occur in Jurassic radiolarites deposited on oceanic crust formed during the opening of the Tethys ocean (Trümpy 1980). These deep-sea exhalative deposits, which are similar to those forming today near active mid-oceanic ridges (*e.g.*, Bonatti 1975), were subsequently metamorphosed during the Alpine orogeny. Several of these radiolarite-hosted deposits contain abundant As and Sb minerals, but Be minerals are extremely rare (Table 1).

The radiolarite-hosted Mn deposits are geologically very different from the Fe–Mn deposits occurring in Val Ferrera, in Graubünden, Switzerland. The latter are dominated by Fe ores (hematite) and are interbedded in Triassic dolomite marbles formed through the metamorphism of sediments deposited on a shallow marine continental platform. Recent petrological and mineralogical investigations, however, have led to the discovery of various As, Sb, Be, and V minerals in several of the Val Ferrera deposits (Brugger 1996, Brugger & Berlepsch 1996, 1997, Brugger *et al.* 1997, 1998). Some of these minerals occur in the main schistosity S_1, which developed under greenschist-facies conditions; examples include medaite $(Mn,Ca)_6(V,As)Si_5O_{19}(OH)$, långbanite $(Mn^{2+},Ca)_4(Mn^{3+},Fe^{3+})_9Sb^{5+}O_{16}(SiO_4)_2$, and barylite $(BaBe_2Si_2O_7)$. Other As, Sb, and V minerals are found in discordant veins cutting the S_1 schistosity; in one of the Val Ferrera deposits, the Fianel mine, an association of Be–Mo–W–(As,Sb,*REE*) minerals occurs in late veins and in the pressure shadow of clasts (Brugger *et al.* 1998).

TABLE 1. SELECTED META-RADIOLARITE HOSTED Mn DEPOSITS FROM THE ALPS

Name	Metamorphic grade	Literature	Mineralogy of As (±V), Sb, Be
Falotta–Parsettens, Graubünden, Switzerland	Zeolite facies	Geiger (1948)	Rich association of arsenates, Sb in tripuhyite. One crystal of bergslagite (Graeser 1995) only.
Val Graveglia, Liguria, Italy	Green-schist facies	Cortesogno *et al.* (1979)	Rich association of vanadates and arsenates. No Be or Sb mineral reported so far.
Praborna, Val d'Aosta, Italy	Eclogite facies	Martin-Vernizzi (1984)	Type locality of roméite. First occurrence of Sb-rich rutile and Sb-rich titanite (Perseil 1991). No Be mineral so far, but titanite and apatite contain some As (Perseil & Smith 1996).

In this communication, we describe a mineral assemblage discovered in pink muscovite – aegirine – hematite – albite schists from the Starlera Fe–Mn mine in Val Ferrera. From a petrological point of view, these schists are valuable because the As, Sb, Be, and V minerals occur as rock-forming minerals, and several stages of element mobility can be distinguished. Most metamorphosed Fe–Mn deposits retain little information about the history of As, Sb, and Be mobility between peak metamorphism and the formation of the late veins. Therefore, the mineral assemblage of the pink schists offers a rare opportunity to gain information about this time span. Furthermore, the pink schists contain titanite, rutile, and roméite with highly unusual compositions. Study of the correlations among the elements present in these minerals allows us to recognize the major mechanisms of substitution, and to extend our knowledge of the crystal chemistry of these minerals.

Methods of Investigation

Petrographic studies were carried out on polished 30-μm thin sections. X-ray powder-diffraction patterns of unknown minerals were obtained using a Gandolfi camera (114.6 mm in diameter). Even small grains (about 100 × 50 × 30 μm) scraped from thin sections can be reliably identified with this method.

Quantitative chemical analyses were carried out with a JEOL JXA–8600 electron microprobe (EMP) at the Institute for Mineralogy and Petrography, University of Basel. Analytical conditions and standards used are given in Table 2. Under the chosen conditions, which allow quantification of the concentration of some minor elements in apatite, it was necessary to scan the beam over a surface of approximately 11 × 8 μm to avoid significant variation of fluorine counts during the measurement (Stormer *et al.* 1993). However, owing to the small size of some apatite grains, some samples had to be analyzed at a higher magnification.

Regional Geology

Val Ferrera, a high valley in canton Graubünden, Switzerland, belongs geologically to the Middle Penninic domain (Briançonnais) of the Eastern Swiss Alps, which is characterized by shallow-water sediments of Triassic to Middle Jurassic age (Trümpy 1980). The Triassic dolomite marbles in Val Ferrera contain numerous small Fe and Fe–Mn deposits, which were intensively mined for Fe from the 14th to the 19th century. An early (syngenetic to diagenetic) origin of these deposits is indicated by the presence of ore pebbles

in Mesozoic sedimentary breccias (precise age unknown; Liassic to Cretaceous: Baudin *et al.* 1995, Schmid *et al.* 1997). Textural and geochemical evidence suggests a sedimentary-exhalative origin (Stucky 1960, Brugger 1996).

During an early stage of the Alpine orogeny, the Triassic carbonate platform was sliced into several tectonic units, now represented by the Middle Penninic Tambo, Suretta, Starlera, and Schams nappes (Baudin *et al.* 1995, Schmid *et al.* 1997). Subsequently, metamorphism evolved from possible blueschist-facies conditions to a greenschist-facies stage (400–450°C, 35–40 Ma; Hurford *et al.* 1989, Brugger 1996); the latter was associated with intense deformation (Ferrera phase, D_1), which produced a pervasive schistosity (S_1). The second phase of deformation (Niemet phase, D_2) also occurred under greenschist-facies conditions and, like D_1, is associated with isoclinal folding. An axial plane schistosity (S_2), however, developed only in the most incompetent rock types. By using the phengite geobarometer of Massonne & Schreyer (1987), Baudin & Marquer (1993) inferred that a decompression of at least 5 kbar took place between D_1 and D_2. The Bergell granodiorite, dated at 30.13 ± 0.17 Ma (von Blanckenburg 1992), cuts D_2 structures and therefore sets a minimum age for D_2 (Liniger 1992). Deformation phase D_3 produced a fine crenulation in the most incompetent rocks. The last event, D_4, occurred under brittle conditions, and was responsible for the formation of subvertical N–S-striking faults.

TABLE 2. ANALYTICAL CONDITIONS FOR ELECTRON-MICROPROBE ANALYSIS

Mineral	kV	nA	Mag[1]	Element-line (standard) [counting time in seconds][2]
Apatite	15	20	10–30 k	P*Kα* and Ca*Kα* (fluorapatite), F*Kα* (topaz)[3], As*Lα* (adamite) [30], Sr*Lα* (strontianite) [30], Na*Kα* (albite), V*Kα* (V_2O_5 synthetic), Ce*Lα* (CeO_2 synthetic) [60], Mn*Kα* (graftonite), Fe*Kα* (graftonite), Si*Kα* (orthoclase).
Hematite	15	50	40 k	Fe*Kα* (hematite), Al*Kα* (sillimanite) [60], Ti*Kα* (rutile) [60], As*Lα* (adamite) [120], V*Kα* (V_2O_5 synthetic) [60], Sb*Lα* (valentinite) [180].
Silicates	15	20	20 k	Si*Kα* (jadeite), Al*Kα* (orthoclase), K*Kα* (orthoclase), Ti*Kα* (rutile), Sb*Lβ* (valentinite) [180], V*Kα* (V_2O_5 synthetic), As*Lα* (adamite), Mg*Kα* (olivine), Ca*Kα* (wollastonite), Fe*Kα* (graftonite), Mn*Kα* (graftonite), Na*Kα* (albite), F*Kα* (topaz) [30][3].
Rutile Titanite	15	20	point	As*Kα* (adamite) [30], Ce*Lα* (CeO_2 synthetic) [40], Sb*Lβ* (valentinite), Nb*Lα* (metallic Nb), W*Lα* (scheelite), other elements, like "Silicates".

Notes: ZAF-type correction was applied to all analytical results. (1) The analyses were performed with a tightly focused beam in scanning mode; a magnification of 20000 × (as passed to the controlling software) corresponds to a scanned surface of 5.5 × 4 μm. (2) If not stated, counting time was 20 s. The counting time applies to the peak and both background measurements. (3) Measured using a LDE1 analyzing crystal.

The Starlera Deposit

Starlera is the only mineral deposit in Val Ferrera that has been exploited for Mn (from 1917 to 1920). The orebody is interbedded within dolomitic marbles but is locally in direct contact with augen gneisses of the underlying basement. Mn ores at Starlera are relatively poor in Si; braunite is the main ore mineral, and the Mn silicates rhodonite and spessartine are absent. Fine needles of romanèchite, $(Ba,H_2O)_2Mn_5O_{10}$, are present along the boundary of braunite grains. The ore contains numerous discordant roméite–tilasite veins, which are up to 30 cm thick and display an unusual assemblage of F-dominant roméite octahedra (≤ 5 mm), coarse-grained tilasite ($CaMgAsO_4F$), idiomorphic aegirine, calcite, phlogopite, and fluorite (Brugger *et al.* 1997).

Tilasite is also present in some hematite – carbonate – quartz ores that occur between the Mn ores and the carbonate wallrocks. These hematite – carbonate – quartz ores display a banded to lenticular texture, with tilasite constituting the main mineral in some of the lenses, which are up to 3 × 0.5 cm in size.

Petrographic Features of the Pink Schists

Interbedded with the Mn ores at Starlera are quartz-rich pink muscovite – aegirine – hematite – albite schists (hereafter referred to as "pink schists"). Aegirine occurs as porphyroblasts that overgrew S_1 and subsequently were deformed by D_3. The latter event is responsible for the pronounced crenulation cleavage (S_3) exhibited by these mica-rich rocks. The pink schists contain abundant rounded grains of zircon showing oscillatory zonation (visible by cathodoluminescence), and two varieties of hematite: (i) fine-grained hematite occurs within the S_1 schistosity, and (ii) coarser-grained hematite is present as spherical aggregates (up to 2 mm in diameter), which were rotated during D_1. In addition, the schists contain titanite, rutile, pyrophanite, roméite, fluorapatite, and bergslagite [$CaBeAsO_4(OH)$]; the association of elements found in these minerals, in particular As, Sb, Ti, F, is related to that in the discordant roméite–tilasite veins. Titanite occurs as chemically heterogeneous crystals (up to 150 μm across; Figs. 1a, b, c), which grew over the main schistosity, and thus after D_1. The crystallization of titanite, however, preceded the last stages of deformation, as shown by the abundance of fractured crystals. Rutile, pyrophanite, and roméite appear in the cracks of broken crystals of titanite (Fig. 1a), and therefore must be younger. Similarly,

formation of at least some of the fluorapatite and bergslagite may postdate the crystallization of titanite, but the textural relationships are less conclusive (Fig. 1b).

The minerals rutile, pyrophanite, roméite, fluorapatite, and bergslagite do not only occur in association with titanite. Rutile is also present as isolated round grains (<100 μm in diameter) in the muscovite matrix, and as sagenitic crystals within aegirine (Fig. 1d). Pyrophanite occurs as isolated inclusions in muscovite, and as a reaction rim around or as topotactic needles within rutile. Roméite forms small (up to 50 μm across), commonly euhedral crystals within the white mica matrix; one crystal also was found enclosed by aegirine, but it is unclear whether such roméite is actually overgrown by pyroxene. Fluorapatite appears in association with bergslagite, with textures suggesting that the two minerals crystallized contemporaneously (Fig. 1e); it further occurs as isolated, typically zoned crystals in the muscovite matrix (Fig. 1f). Bergslagite, which is uniformly associated with fluorapatite, clearly overgrows S_1, and may have crystallized at the same time as aegirine (Fig. 1e).

Mineral Chemistry

The main minerals occurring in the pink schists at Starlera display distinctive chemical features (Table 3).

TABLE 3. COMPOSITION OF MUSCOVITE AND AEGIRINE, PINK SCHIST, SAMPLE JB345, STARLERA

	Muscovite			Aegirine		
	Average	Min	Max	Average	Min	Max
n	18			8		
SiO_2	50.41	49.62	52.96	54.69	54.23	55.99
TiO_2	0.44	0.13	0.80	0.24	<0.04	0.70
Al_2O_3	19.80	19.10	21.22	3.12	2.54	4.26
V_2O_5	0.03	<0.03	0.05	n.a.		
FeO				1.49	0.60	2.67
Fe_2O_3	6.77	6.28	7.68	24.27	16.15	21.01
MnO	0.82	0.59	1.03	1.24	0.88	1.71
MgO	4.33	4.06	4.77	1.95	1.60	2.86
CaO	0.02	<0.02	0.17	2.97	2.34	4.26
Na_2O	0.08	0.05	0.12	11.97	11.02	12.47
K_2O	12.14	11.82	12.35	<0.05	<0.05	0.08
BaO	0.24	<0.05	0.54	n.a.		
F	<0.05			n.a.		
Sum	95.04			101.95		
H_2O_{calc}	4.34					
Sum	99.38					

Note that the normalization for muscovite is based on $Fe^{3+} = Fe_{total}$, 10 atoms of oxygen and 2 (OH) per formula unit: $(Si_{3.483}Al_{0.517})(Al_{1.095}Mg_{0.446}Fe^{3+}_{0.325}Mn_{0.048}Ti_{0.023})(K_{1.070}Na_{0.011}Ba_{0.006})O_{10}(OH)_2$.

The normalization for aegirine is based on four cations and Fe^{3+}/Fe^{2+} calculated for a total of six atoms of oxygen per formula unit: $Si_{2.018}(Fe^{3+}_{0.674}Al_{0.135}Mg_{0.100}Fe^{2+}_{0.046}Mn_{0.039}Ti_{0.007})(Na_{0.850}Ca_{0.123}Mg_{0.010})O_6$.

The mica is rich in Fe^{3+} and Mg, and its composition is intermediate between a hypothetical ferrian muscovite end-member $K(AlFe^{3+})(Si_3Al)O_{10}(OH)_2$ and aluminoceladonite $K(AlMg)Si_4O_{10}(OH)_2$; furthermore, the mica contains significant amounts of Ti (up to 0.80 wt% TiO_2) and Mn (up to 1.03 wt% MnO), but is poor in Na, Ba and V; both F and Sb contents are below EMP detection limits (F < 0.05 wt%; Sb < 200 ppm). The aegirine porphyroblasts (67.4 mole % aegirine component, on average) contain, like muscovite, considerable amounts of Ti and Mn (to 0.70 wt% TiO_2 and 1.71 wt% MnO), and lack detectable Sb (less than 0.03 wt% Sb_2O_5). Albite is very pure, containing less than 0.03 wt% CaO and less than 0.20 wt% BaO.

Pyrophanite

All analyzed crystals of pyrophanite contain significant amounts of Sb, ranging from 0.97 to 1.91 wt% Sb_2O_5 (Table 4). This elevated concentration of Sb can mainly be attributed to the exchange vector

$$Sb^{5+}Fe^{3+}Ti^{4+}_{-2} \quad (1),$$

which defines the solid solution between pyrophanite, $MnTiO_3$, and melanostibite, $Mn(Sb^{5+},Fe^{3+})O_3$ (Moore 1968). Exchange vector (1) can be generalized as:

$$Me^{5+}Me^{3+}Ti^{4+}_{-2} \quad (2).$$

Although two types of pyrophanite can be distinguished on a textural basis (isolated grains within muscovite and pyrophanite replacing rutile), they have very similar chemical compositions, suggesting that all the pyrophanite grains may have formed by replacement of former grains of rutile.

Rutile

The presence of Sb^{5+} in rutile-related structures is documented by the minerals squawcreekite (Fe,Sb,Sn,Ti)O_2 (Foord *et al.* 1991) and tripuhyite (Hussak & Prior 1897, Mason & Vitaliano 1953). The chemical formula of tripuhyite is still reported as $Fe^{2+}Sb^{5+}_2O_6$ in some compilations (*e.g.*, Blackburn & Dennen 1997), despite solid evidence for the formula $Fe^{3+}Sb^{5+}O_4$ as suggested originally by Mason & Vitaliano (1953). In particular, Mössbauer spectroscopy attests the trivalent oxidation state for Fe in natural tripuhyite (Gakiel & Malamud 1969).

The empirical chemical formulae (Fe,Sb,Sn,Ti)O_2 with Fe ≈ Sb >> (Sn+Ti), and $Fe^{3+}Sb^{5+}O_4$ for squawcreekite and tripuhyite, respectively, are identical, but the minerals must have different structures. However, no structure refinement is available for these minerals, because of the lack of suitable single crystals. Squawcreekite is reportedly isostructural with rutile (*i.e.*, disordered substitution of Fe and Sb in the Ti site).

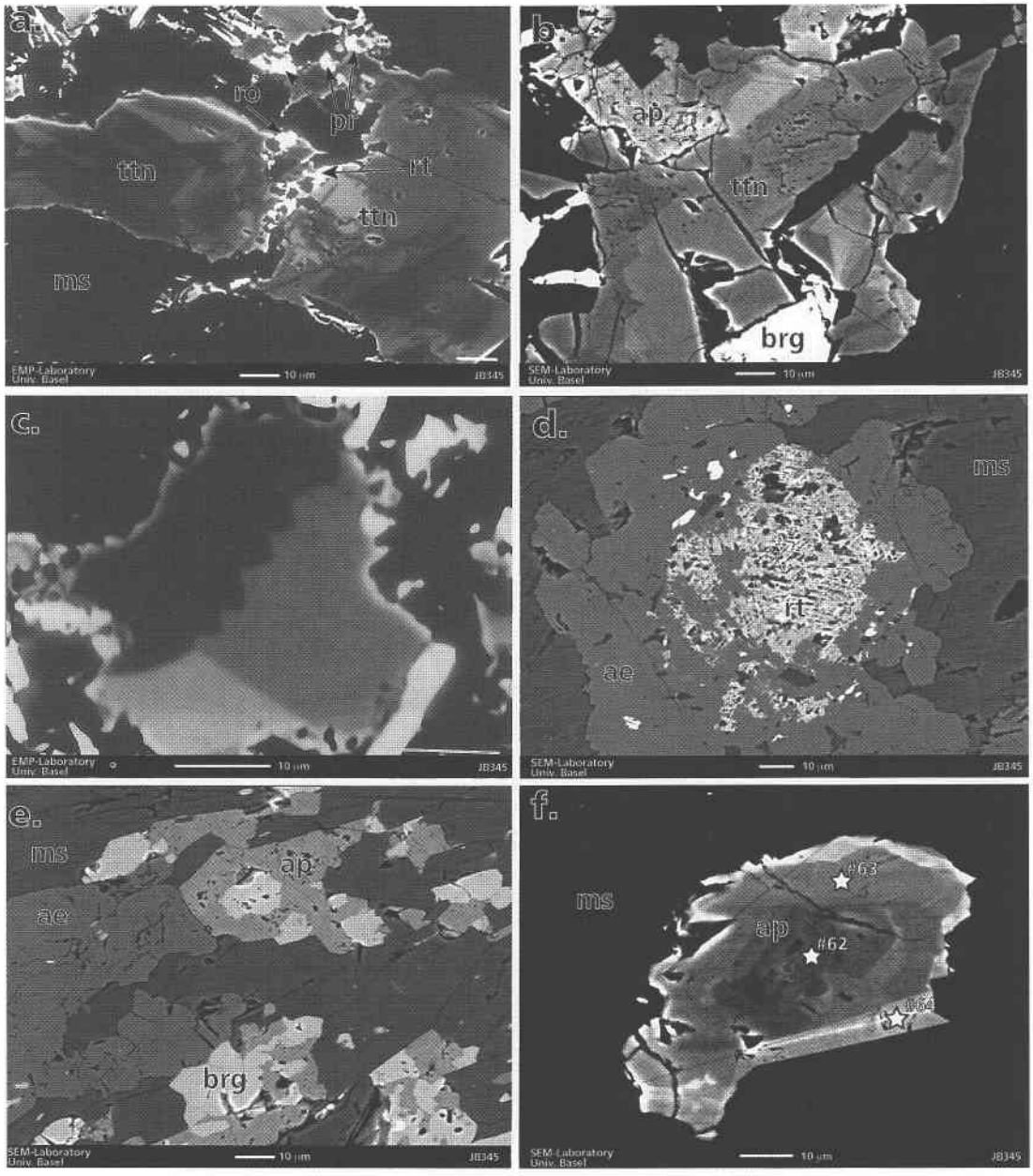

FIG. 1. BSE pictures illustrating the zonation and textures of the minerals in the pink schists from Starlera. (a) Broken crystal of titanite; sample JB345.C2. (b) Association of titanite, fluorapatite and bergslagite; sample JB345.C8. (c) Titanite crystal displaying zonation with three sectors; sample JB345.C2. (d) Antimonian rutile found inside a crystal of aegirine; sample JB345.C7. (e) Textural relations between fluorapatite and bergslagite; sample JB345.C13. (f) Zoned crystal of fluorapatite; sample JB345.C2. The location of three EMP analyses (#62, 63, 64) is indicated (*cf.* Table 7, Fig. 7). Abbreviations: *ae*: aegirine, *ap*: fluorapatite (light gray: As-rich), *brg*: bergslagite, *hem*: hematite, *pr*: pyrophanite, *ro*: roméite, *rt*: rutile, *ttn*: titanite (light gray: Sb-rich).

TABLE 4. COMPOSITION OF RUTILE, PYROPHANITE, TITANITE AND ROMEITE FROM THE PINK SCHISTS AT STARLERA

Analysis #	1	2	3	4	5	6	7	8	9	10	11	12	13
	Rutile				Pyrophanite		Titanite				Roméite-betafite		
n=	1	1	1	1	3	3	1	1	1	27	1	1	19
SiO_2	n.a.	n.a.	n.a.	n.a.	n.a.	n.a.	28.01	27.84	29.70	28.01-30.86	n.a.	n.a.	n.a.
TiO_2	100.06	54.17	73.75	85.89	52.33	51.81	28.36	33.22	35.38	28.36-37.92	14.16	21.49	14.16-23.00
Al_2O_3	n.a.	n.a.	n.a.	n.a.	n.a.	n.a.	1.30	1.25	0.82	0.82-1.38	n.a.	n.a.	n.a.
Sb_2O_5	0.05	30.63	15.94	8.22	1.05	1.57	9.55	3.01	2.12	0.47-9.55	47.51	30.25	30.25-47.51
V_2O_5	0.48	0.23	0.49	0.52	0.22	0.21	0.11	0.41	0.16	<0.05-0.41	0.16	0.18	<0.04-0.18
As_2O_5	n.d.	0.54	<0.05	<0.05	<0.05	<0.05	1.67	3.46	0.81	0.57-3.46	<0.05	<0.05	<0.05
Nb_2O_5	0.41	0.63	1.33	0.63	0.30	0.36	0.20	0.18	0.70	<0.04-0.84	1.04	1.18	0.59-2.13
WO_3	0.22	0.10	<0.05	0.16	0.21	0.04	0.12	0.18		<0.05-0.22	1.10	1.83	0.44-1.83
CaO	<0.03	0.03	0.77	0.03	<0.03	<0.03	24.76	25.53	26.72	24.74-27.56	16.35	11.69	11.69-16.35
Na_2O	<0.03	<0.03	<0.03	0.05	<0.03	<0.03	0.70	0.45	0.17	0.06-0.77	1.66	0.38	0.31-2.26
MnO					45.83	46.50					3.76	7.04	3.76-7.61
Fe_2O_3	0.74	15.66	8.54	4.96	0.65	1.49	3.03	3.06	1.89	1.27-3.08	0.44	0.24	0.22-1.66
Mn_2O_3	0.27	1.09	0.51	0.65			1.30	1.68	0.60	0.53-1.68			
Ce_2O_3	<0.04		0.09	<0.04	<0.04	n.a.	<0.04	<0.04	0.20	<0.04-0.28	11.63	23.90	11.63-23.90
F	n.a.	n.a.	n.a.	n.a.	n.a.	n.a.	<0.05	<0.05	<0.05	<0.05	2.04	0.31	0.28-2.53
-(O=F)											0.86	0.13	
Sum	102.23	103.08	101.42	101.10	100.59	101.98	99.11	100.27	99.27	99.00-101.25	98.99	98.36	95.67-98.60
Si^{4+}							0.971	0.934	0.994	0.965-1.002			
Ti^{4+}	0.982	0.622	0.793	0.889	0.990	0.969	0.739	0.839	0.891	0.733-0.932	0.722	1.126	0.729-1.151
Al^{3+}							0.053	0.049	0.032	0.032-0.055			
Sb^{5+}	<0.001	0.174	0.085	0.042	0.010	0.014	0.123	0.038	0.026	0.006-0.123	1.197	0.783	0.783-1.208
As^{5+}		0.004					0.030	0.061	0.014	0.010-0.061			
Nb^{5+}	0.002	0.004	0.009	0.004	0.004	0.004	0.001	0.001	0.004	0.005	0.032	0.037	0.018-0.066
V^{5+}	0.004	0.002	0.005	0.005	0.004	0.004	0.003	0.009	0.004	0.009	0.007	0.008	0.008
Fe^{3+}	0.007	0.180	0.092	0.051	0.014	0.028	0.079	0.077	0.048	0.032-0.79	0.023	0.013	0.011-0.086
Mn^{3+}	0.003	0.013	0.006	0.007			0.034	0.043	0.015	0.013-0.037			
W^{6+}	0.001	<0.001			0.001		0.001	0.002		0.002	0.019	0.033	0.008-0.033
Σ					1.023	1.019	1.063	1.118	1.034	1.030-1.118	2.000	2.000	
Ca^{2+}			0.012				0.919	0.918	0.958	0.908-0.974	1.188	0.872	0.872-1.199
Na^+						0.001	0.047	0.029	0.011	0.004-0.051	0.218	0.051	0.042-0.290
Mn^{2+}					0.977	0.980					0.216	0.415	0.218-0.429
Ce^{3+}									0.002	0.003	0.289	0.609	0.284-0.609
Σ					0.977	0.981	0.966	0.947	0.971	0.959-0.984	1.911	1.947	1.871-2.010
F^-										0.008	0.437	0.068	0.061-0.530
O^{2-}_{calc}	1.999	1.996	1.993	1.993	3.025	3.016	5.004	5.004	5.001	4.985-5.018	6.353	6.634	6.237-6.646

Notes: The above compositions, expressed in weight %, are results of electron-microprobe analyses. Normalization procedures for rutile: Σ(cations) = 1. For pyrophanite, Σ(cations) = 2. For titanite, Σ(cations) = 3. For roméite–betafite, Σ(Sb,Ti,Fe,Nb,V,W) = 2. Column headings: 1) isolated rutile in muscovite, 2) rutile with the highest Sb_2O_5 content (selected from a total of nine analyses, sample JB345A.11), 3) rutile from sample JB345.C2 (*cf.* Fig. 1a), 4) rutile (sagenitic) in core of a pyroxene porphyroblast (*cf.* Fig. 1d), 5) pyrophanite, isolated grains in muscovite, sample JB345.C9, 6) pyrophanite, replacing rutile in samples JB345.C3 and JB345.C7 (the associated rutile contains <0.03 wt% Sb_2O_5), 7) Sb-rich titanite, sample JB345.C8, 8) As-rich titanite, sample JB345.C8, 9) selected compositions of titanite from sample JB345.C3, 10) minimum and maximum values for titanite from sample JB345, 11) "roméite" from sample JB345 (corresponding point labeled on Fig. 5), 12) selected composition of "betafite" from sample JB345 (corresponding point labeled on Fig. 5), 13) minimum and maximum values for "roméite–betafite" from sample JB345.

Assignment of a "trirutile" cell (tapiolite group) to tripuhyite relies solely on a relatively weak reflection at d = 4.23 Å on the X-ray powder diagram, which cannot be indexed within a rutile structure (Mason & Vitaliano 1953). A "trirutile" structure, however, implies a compound of the type AB_2O_6; more work is clearly needed to establish the nature of tripuhyite and its relations to squawcreekite. Nevertheless, both minerals illustrate extensive substitution along vector (1) in rutile-like structures.

Perseil (1991) reported the first occurrence of antimonian rutile in the radiolarite-hosted metamorphosed Mn deposits at Praborna, Italy, and suggested the exchange $Sb^{3+}Ti^{3+}_{-1}$ as a possible mechanism for incorporation of Sb. More recently, however, Smith & Perseil (1997) dismissed Ti^{3+}, regarded Sb^{3+} as doubtful, and recognized that exchange vector (1) accounts for most of the chemical variability of the Praborna rutile, which contains up to 33.75 wt% Sb_2O_5 (corresponding to 0.2 Sb atoms per formula unit [*apfu*]). The affinity of rutile for pentavalent cations is well known (*e.g.*, Nb^{5+}, *cf.* Černý *et al.* 1964).

In the pink schists at Starlera, rutile occurs in various microtextural relationships with other minerals, and is chemically distinct in different settings. In the main schistosity S_1, rutile hosts less than 0.1 wt% Sb_2O_5, whereas rutile in late cracks in titanite as well as sagenitic rutile in the core of aegirine porphyroblasts contains up to 30.63 wt% Sb_2O_5. The latter two varieties are also characterized by high Fe contents, and small but commonly significant quantities of As (Table 4). All types of rutile host considerable amounts of Nb, V, and

Mn (to 1.5 wt% of oxides), and some contain in addition minor amounts of W. Figure 2 compares data for rutile from Starlera with data from Praborna. In Figure 2a, Mn has been included as Mn^{3+} to calculate the correlation between Fe + Mn and the pentavalent cations (Me^{5+} = Sb + V + Nb), among which Sb is the most abundant at Starlera ($0.83 < Sb/Me^{5+} < 0.86$). Choice of Mn^{3+} as the predominant form of Mn is consistent with the occurrence of the Mn^{2+}–Mn^{3+} mineral braunite, and with considerations of ionic sizes: the ionic radius of octahedrally coordinated Mn^{3+} (0.64 Å; Shannon 1976) is similar to that of Ti^{4+} (0.60 Å), Fe^{3+} (0.64 Å), and Sb^{5+} (0.60 Å), whereas that of Mn^{2+} (0.83 Å) is significantly larger. The correlations and slopes of the regression lines shown in Figure 2 strongly suggest that exchange vector (2) [with a major component of the vector (1)] is of primary importance in rutile from both localities.

Titanite

The crystal structure of titanite, $CaTi(O,OH,F)SiO_4$, allows for incorporation of a wide range of elements, including U, Th, the rare-earth elements (*REE*), Na, Mn, Fe^{2+}, Fe^{3+}, Mg, Sr, Ba, Nb, Ta, Al, V and Cr (*e.g.,* Deer *et al.* 1982, Gieré 1992, Pan & Fleet 1992, Russell *et al.* 1994, Kunz *et al.* 1997). In addition to these elements, Sb and As have recently been observed in natural titanite. Perseil & Smith (1995) discovered Sb-rich titanite in the Mn ores of Praborna, Italy (up to 12.59 wt% Sb_2O_5), and subsequently also reported the presence of up to 3.5 wt% As_2O_5 in these Sb-rich titanite crystals (Perseil & Smith 1996). Significant amounts of As also are present in hydrothermal titanite from fissures in the Binntal, central Swiss Alps (up to 3.60 wt% As_2O_3; Krzemnicki & Gieré 1996, Krzemnicki 1996). This compositional flexibility of titanite is one of the main reasons why the mineral was proposed as a possible host-phase for high-level nuclear waste (*e.g.,* Hayward 1988).

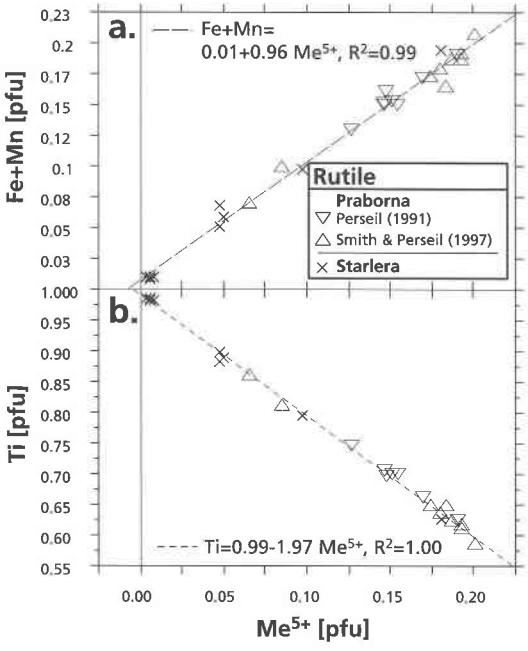

FIG. 2. Plots of (a) (Fe + Mn) *versus* Me^{5+} and (b) Ti *versus* Me^{5+} illustrating the exchange vector $Me^{5+}(Fe^{3+},Mn^{3+})Ti^{4+}_{-2}$ recognized in rutile from Starlera (nine data points [this study]; Me^{5+} = Sb + V + Nb) and Praborna (data from Perseil 1991 and Smith & Perseil 1997; Me^{5+} = Sb). Errors at the 2σ level are smaller than symbols.

In the ores of Val Ferrera, titanite is relatively rare and could only be identified in the pink schists at Starlera. On back-scattered electron (BSE) images, titanite crystals display complex patterns of zoning, which are mainly related to variations in the Sb and Ti contents, with Sb-rich zones appearing brighter (Figs. 1a–c). The zonation commonly represents sector zoning (Fig. 1c), a typical feature in titanite (*e.g.,* Bouch *et al.* 1997, Krzemnicki & Gieré 1996, Krzemnicki 1996, Paterson & Stephens 1992). In some cases, titanite exhibits Sb-rich zones along fractures (Fig. 1a), indicating that Sb was introduced metasomatically.

The most striking characteristic of the titanite from Starlera is that all crystals contain high concentrations of Sb, As, and Mn (Table 4). F was not detected in any crystal (<0.05 wt% F), but low amounts of Na, W, Nb, V, and Ce are generally present. Derivation of the structural formula of this titanite is not a trivial problem, because the H_2O content is unknown, and several elements could occur in more than one oxidation state and at different sites.

In the pink schists at Starlera, Sb is an important constituent of titanite (up to 9.55 wt% Sb_2O_5) and may be present as either Sb^{3+} or Sb^{5+}; the ionic radii suggest that the octahedrally coordinated Ti site (0.60 Å) could easily accommodate Sb^{5+} (0.60 Å) and possibly some Sb^{3+} (0.76 Å), whereas the Ca site (1.06 Å in coordination seven) probably can only host Sb^{3+} (>0.76 Å). Data from the Starlera occurrence display an excellent inverse correlation between Ti and Sb, but no significant correlation between Ca and Sb (Table 5). These relationships strongly suggest that Sb occurs in the Ti site of the titanite structure, most probably as Sb^{5+}. Vanadium, Nb, and possibly As (see below) are other pentavalent cations present in minor amounts in the Starlera titanite. The slope of the regression line for Ti *versus* Me^{5+} (Fig. 3a) is intermediate between the slope associated with exchange vector (2) and that of

$$Na\ Me^{5+}\ Ca_{-1}\ Ti_{-1} \qquad (3),$$

an exchange vector indicated by the correlation matrix given in Table 5. Vector (2), with a large component of

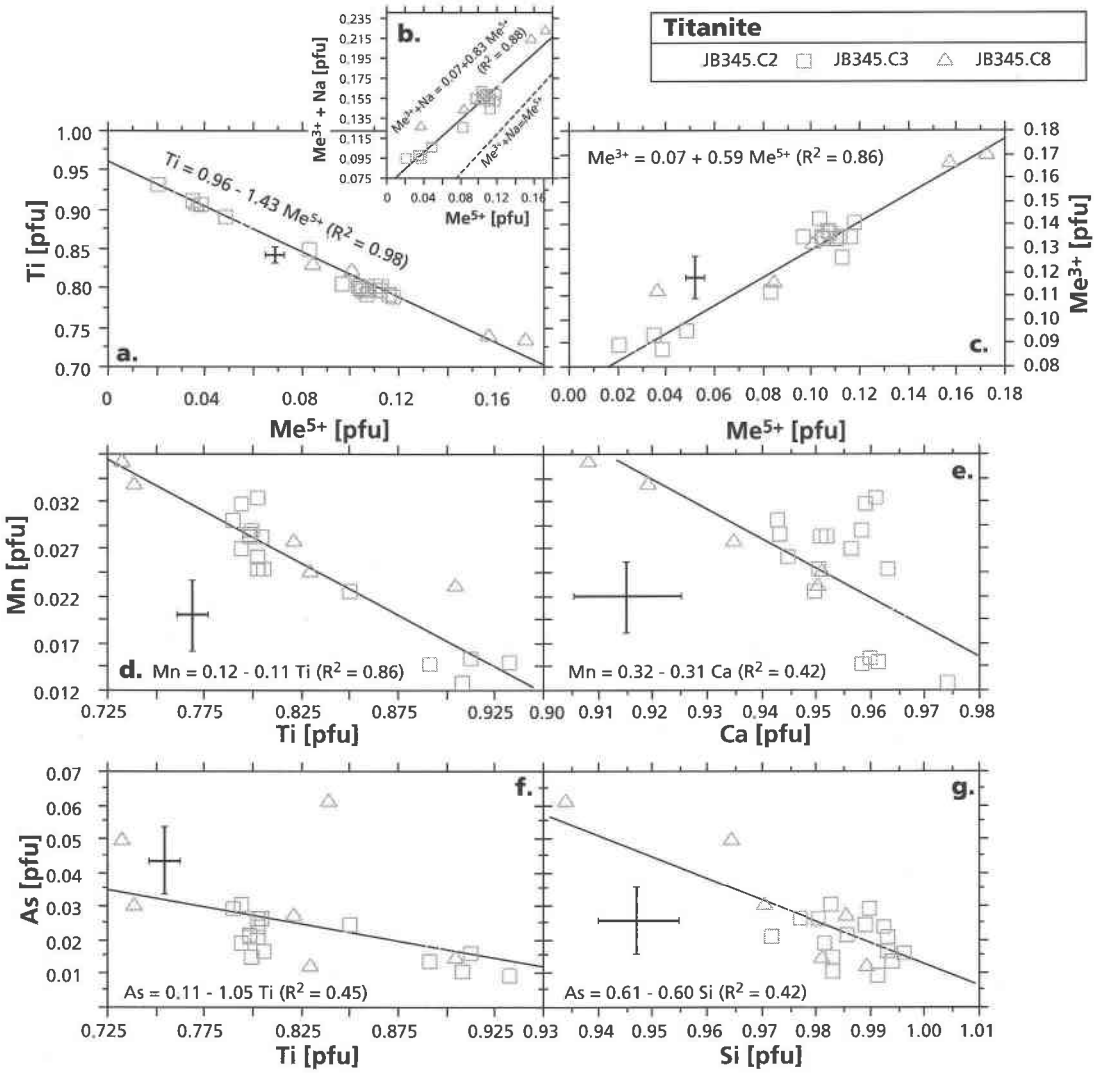

FIG. 3. Diagrams illustrating the crystal chemistry of titanite from the pink schists at Starlera (sample JB345). Error bars correspond to 2σ errors resulting from counting statistics. (a) Ti *versus* Me^{5+}, (b) Me^{3+} + Na *versus* Me^{5+}, (c) Me^{3+} *versus* Me^{5+}, (d) Mn *versus* Ti, (e) Mn *versus* Ca, (f) As *versus* Ti, (g) As *versus* Si. Notes: Me^{3+} = Al + Mn + Fe, Me^{5+} = Sb + As + V + Nb.

vector (1), is predominant in the Praborna titanite (Perseil & Smith 1995), as well as in rutile from Starlera and Praborna (see above). If vectors (2) and (3) account for the substitution of all pentavalent cations, Na + Me^{3+} must be equal to or greater than Me^{5+}. This condition is indeed fulfilled (Fig. 3b). The regression lines indicate that at Me^{5+} = 0, titanite from the pink schists contains some Me^{3+} (Fig. 3c), but no Na. The excess Me^{3+} may be accounted for by the substitution

$$Me^{3+}(OH)\ Ti_{-1}O_{-1} \qquad (4)$$

which is common in titanite (*e.g.*, Gieré 1992). Substitution (4) further explains the intercept at 0.96 instead of 1.00 in the Ti *versus* Me^{5+} diagram (Fig. 3a).

The assignment of most of Fe and Mn as trivalent cations to the Ti site, implicitly assumed in the preceding discussion, is supported by the good negative correlation of each of these elements with Ti (Table 5, Fig. 3d for Mn). This conclusion is also consistent with the generally high oxidation state of the Mn ores and, in addition, with the similar ionic sizes of $^{VI}Mn^{3+}$ (0.64 Å), $^{VI}Fe^{3+}$ (0.64 Å) and $^{VI}Ti^{4+}$ (0.60 Å). However, both Fe

TABLE 5. CORRELATION MATRIX FOR THE MAIN ELEMENTS PRESENT IN THE TITANITE FROM STARLERA

	Na	Ca	Ti	Si	Sb	As	Al	Fe	Mn
Ca	-0.82	1.00							
Ti	-0.83	0.63	1.00						
Si	-0.63	0.32	0.57	1.00					
Sb	0.84	-0.62	-0.99	-0.58	1.00				
As	0.63	-0.65	-0.67	-0.65	0.66	1.00			
Al	0.51	-0.45	-0.72	-0.51	0.69	0.57	1.00		
Fe	0.88	-0.76	-0.94	-0.55	0.92	0.63	0.64	1.00	
Mn	0.77	-0.65	-0.93	-0.60	0.90	0.61	0.74	0.92	1.00
Me^{3+}	0.82	-0.71	-0.95	-0.60	0.93	0.66	0.81	0.96	0.97

Notes: n = 26; the most As-rich composition (anal. #8, Table 4) has been omitted because it is in many cases distinct from other compositions, and thus exerts a large influence on the linear regressions. Me^{3+} = Al + Fe + Mn; based on normalized electron-microprobe data.

and Mn also display a negative, though poorer correlation with Ca (Table 5, Fig. 3e for Mn), and the cation totals are systematically greater than unity for the Ti site, if the total amounts of Fe and Mn are assigned to the Ti site (Table 4). We therefore conclude that Mn and Fe occur primarily as trivalent cations at the Ti site, but to some extent as divalent cations at the Ca site as well. A similar situation was reported for the Sb-rich titanite from Praborna (Perseil & Smith 1995). At Starlera, however, titanite displays higher Mn contents (maximum 1.68 wt% Mn_2O_3) than at Praborna (1.10 wt%; Mottana & Griffin 1979). The presence of Fe^{3+} (along with Al^{3+}) at the Ti site is very common in titanite, and is documented from diverse geological environments; a review was provided by Gieré (1992).

The concentration of As in titanite from Starlera varies considerably and may be as high as 3.46 wt% As_2O_5 (Table 4). Arsenic commonly is present in minerals as either As^{3+} (in arsenites) or As^{5+} (in arsenates). In titanite, As^{5+} could substitute for Si in the tetrahedral sites; this is the case, for example, in the silico-arsenate mineral cervandonite-(Ce) (Armbruster *et al.* 1988). The ionic radius of As^{3+} (0.58 Å) is very similar to that of octahedrally coordinated Ti^{4+} (0.60 Å) and thus, the Ti site most likely accommodates As as As^{3+}. However, the Ti site may also be able to host the smaller As^{5+} ion (0.46 Å). For the Starlera titanite, As exhibits inverse (albeit poor) correlations with both Si and Ti (Figs. 3f, g, Table 5). The quality of the correlation is affected by the fairly large analytical error for As and by the fact that As is only a minor component. Nevertheless, these data are compatible with the occurrence of As in both the Si and Ti sites. An inverse correlation is also observed between As and Ca (Table 5), which could be explained by the coupled substitution:

$$Na^{[IV]}As^{5+}Ca_{-1}Si_{-1} \quad (5)$$

The high oxidation state of the Starlera ores and the association of titanite with arsenate minerals (bergslagite, tilasite) suggest that As occurs primarily as As^{5+}. In contrast, the trivalent oxidation state has been inferred for As contained in the titanite from Binntal; it is associated with arsenite minerals, and accommodates As in the Ti site (Krzemnicki & Gieré 1996, Krzemnicki 1996). The crystal chemistry of As in the Starlera titanite is therefore different from that of the Binntal, with As occurring as As^{5+} in the Ti and Si sites at Starlera.

The composition of titanite at Starlera can be simplified and described in terms of the seven components Ca, Na, Ti, Si, Me^{3+} (*i.e.*, Al, Fe, Mn), Me^{5+} (*i.e.*, Sb, As, Nb, V), O, and OH. If we neglect the small amounts of As^{5+} inferred to be present in the Si site and the minor amounts of Fe^{2+} and Mn^{2+} possibly occurring in the Ca site, we can define the composition space by four end-members (Fig. 4a), emphasizing the deviation from the ideal composition $CaTiOSiO_4$: (A) $CaTiOSiO_4$ [origin], (B) $Ca(Me^{3+}_{0.5}Me^{5+}_{0.5})OSiO_4$ [vector (2)], (C) $CaMe^{3+}OHSiO_4$ [vector (4)], and (D) $NaMe^{5+}OSiO_4$ [vector (3)]. As shown in Figures 4b and 4c, end-member D is of minor importance, and the compositional variability is mainly due to substitution along vector (2), a result that was also found for titanite at Praborna (Perseil & Smith 1995). At Starlera, vector (2) is therefore responsible for incorporation of Sb in three Ti minerals (pyrophanite, rutile, and titanite). Note that vector (4) represents a maximum OH content (all Mn and Fe assumed to be trivalent), and is associated with a large cumulative error; for these reasons, calculated H_2O contents are not reported in Table 4.

Roméite

Roméite, $^{[A]}(Ca,Na,Ce,\square)_2{}^{[B]}(Sb,Ti)_2O_6(F,OH,O)$, can be regarded as a member of the pyrochlore group (Hogarth 1977). It occurs as an accessory mineral in metamorphosed syngenetic-exhalative Mn deposits and in hydrothermal veins. Brugger *et al.* (1997) described several occurrences of roméite in Val Ferrera, including the roméite–tilasite veins from Starlera. The composition of roméite from the pink schists, however, is distinct from that of all previously investigated samples, primarily because of its unusually high Ce contents, which range from 11.63 to 23.9 wt% Ce_2O_3 (Table 4). To our knowledge, these are by far the highest Ce contents ever reported for this mineral; they are significantly higher than those observed at all other localities in Val Ferrera, where 4.22 wt% Ce_2O_3 was found as a maximum concentration (Brugger *et al.* 1997). The Ce:Ca ratio reaches a value of 0.7 (Fig. 5), such that Ce is not far from being the dominant *A*-site cation. Moreover, the roméite occurring in the pink schists at Starlera is Ti-rich, with the amount of Ti in *apfu* exceeding that of Sb in several grains; the latter should, strictly speaking, be named antimonian betafite (Fig. 5). Antimonian betafite has also been observed in the Fe–Mn deposit at Fianel (Brugger *et al.* 1997), where it rarely occurs as a core in zoned roméite. These cores of antimonian betafite, however, contain high amounts of U and H_2O, a feature characteristic of betafite, but that is not observed in samples from the pink schists at Starlera.

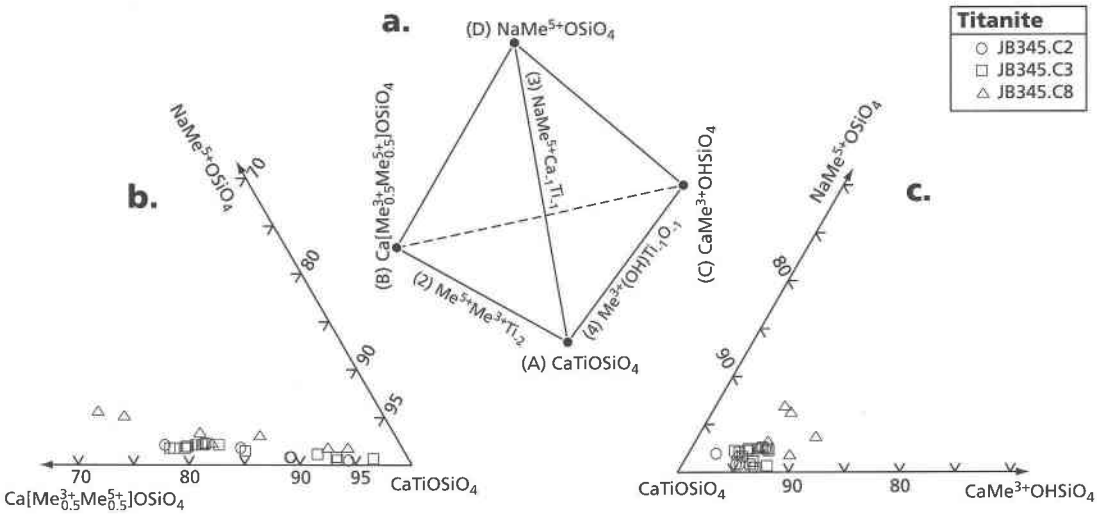

FIG. 4. (a) Tetrahedron illustrating the various end-members and exchange vectors allowing the incorporation of trivalent or pentavalent cations (or both) at the octahedrally coordinated Ti site of titanite. (b) Projection of the compositions from Starlera on (A)–(B)–(D). (c) Projection of the compositions from Starlera on (A)–(C)–(D). The proportion of the end-members was calculated from the compositions normalized to three cations (in *apfu*) according to the following assumptions: Na = (D), Me^{5+} = 0.5(B) + (D), Me^{3+} = 0.5*(B) + (C), (A) + (B) + (C) + (D) = 1. Notes: Me^{3+} = Al + Mn + Fe, Me^{5+} = Sb + As + V + Nb.

Figure 6a illustrates the one-for-one replacement of Ti by Sb, expressed in mole of element/(100 g mineral) to avoid artifacts introduced by normalization of the chemical results. A recent crystal-structure refinement revealed that in some samples of roméite from Praborna (type locality of roméite; Damour 1841), the Mn content is split into two sites, *i.e.*, as Mn^{2+} in the *A* site and as Mn^{3+} in the *B* site (R.C. Rouse, written commun. 1997). At Starlera, the very good inverse correlation between Ca and Mn (Fig. 6b) suggests that most Mn occurs as Mn^{2+} at the *A* site, in accord with the substitution

$$^{[A]}Mn^{2+}\ ^{[A]}Ca_{-1} \quad (6).$$

Ce and Ti exhibit an excellent positive correlation (Fig. 6c, Table 6), which is consistent with the exchange vector (Brugger *et al.* 1997):

$$Ce^{3+}Ti^{4+}_{2}\ Na^{+}_{-1}Sb^{5+}_{-2} \quad (7).$$

Vector (7) also conforms with the relationship between Sb and Ti (Fig. 6a). This vector accounts for the all the Ce contained in the roméite samples described by Brugger *et al.* (1997). For the roméite occurring in the pink schists, however, the slope of the linear fit in Figure 6c is closer to +1.0 than to +0.5, and an additional exchange-vector must therefore be operating to account for the incorporation of all Ce into roméite. A possibility that does not affect the Ti content is the substitution

$$CeO\ Ca_{-1}F_{-1} \quad (8),$$

as suggested by the correlation data given in Table 6. If vectors (7) and (8) operate simultaneously, we can describe the incorporation of Ce into roméite by the overall substitution

$$Ce_2Ti_2ONa_{-1}Ca_{-1}Sb_{-2}F_{-1} \quad (9),$$

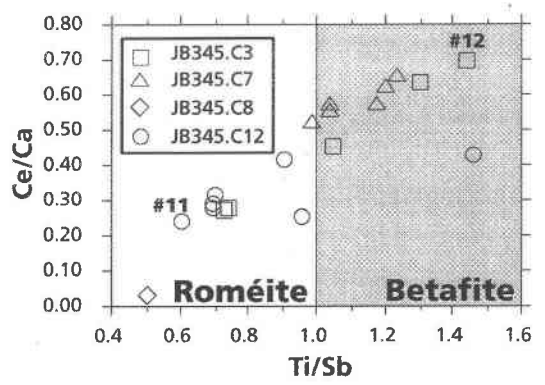

FIG. 5. Nomenclature diagram for roméite–betafite. Chemical compositions of the two labeled points are listed in Table 4.

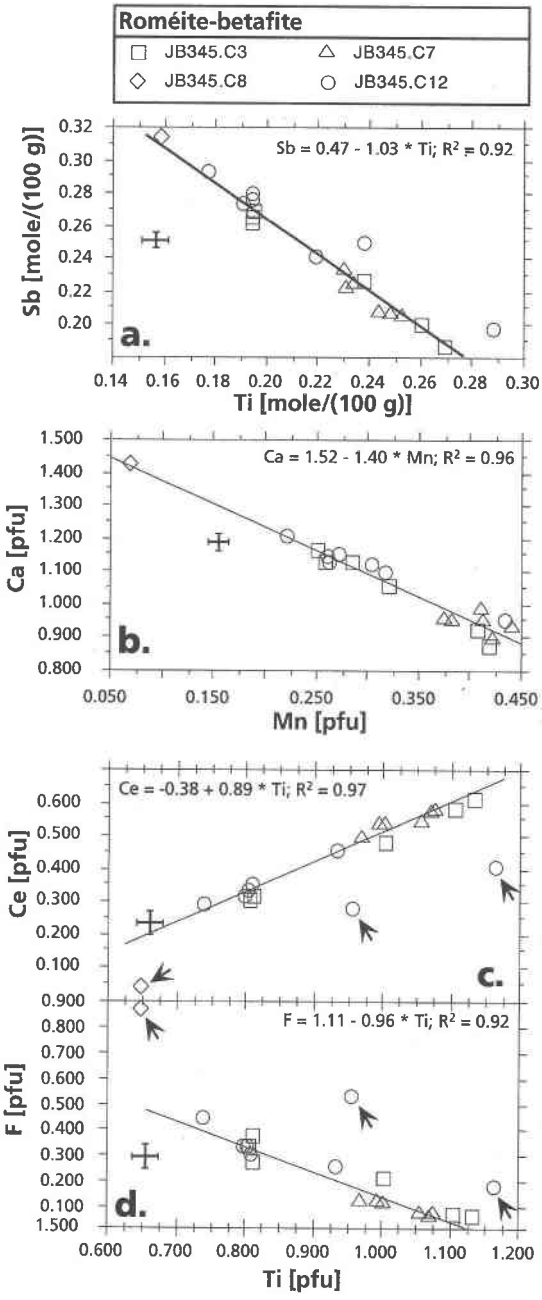

FIG. 6. Element correlations for roméite–betafite from the pink schists at Starlera (sample JB345). (a) Sb *versus* Ti (in units of moles Sb [Ti] per 100 g of mineral), (b) Ca *versus* Mn, (c) Ce *versus* Ti, (d) F *versus* Ti. In Figures 6c and 6d, the regression lines were calculated without the three data points marked by arrows (see text). Error bars correspond to 2σ and result from counting statistics.

which accounts for the slopes of the Ce/Sb (–0.87), Sb/Ti (–1.03, Fig. 6a), and Na/Sb (0.52) regression lines. Equation (9) predicts a slope of approximately –0.5 for the regression line between F and Ti. The observed slope of –0.96 (Fig. 6d) can be explained by allowing the F content to vary along the additional exchange-reaction

$$(OH)F_{-1} \qquad (10).$$

Given the many cations that enter the structure of roméite along various independent exchange-vectors, it is surprising that the correlations between each pair of elements (Table 6) are still excellent. Three datasets have been omitted in the calculation of the linear regression; these data points define an independent array that is nearly parallel to the main trend (*e.g.*, Figs. 6c, d). The correlations of Table 6 imply that the substitutions (6), (7), (8), and (10) operate simultaneously in these samples of roméite. As no crystal-chemical reason apparently explains the link among the various independent exchange-vectors, an external control by fluid chemistry seems likely.

Fluorapatite

Many elements can enter the structure of fluorapatite, $Ca_5(PO_4)_3F$; for apatite occurring in Mn deposits, the most significant among these are: Sr, Mn, Fe, and Ce at the two *Ca* sites; As, Si, and possibly $(CO_3)^{2-}$ at the *P* site, and $(OH)^-$ at the *F* site.

In the pink schists at Starlera, fluorapatite is present as isolated grains and locally, it exhibits a complex chemical zonation (Fig. 1f). This pronounced zoning is mainly the result of highly variable As contents (2.2–13.8 wt% As_2O_5; *cf.* Table 7) which, as shown in Figure 7a, can be explained by the simple substitution $As^{5+}P_{-1}$. In general, the As content of apatite at Starlera increases toward the edge of the crystals. In BSE images, the zoned crystals commonly display two distinct stages of growth, whereby As-rich apatite (stage 2) appears along fractures within or as a rim around apatite of stage 1 (see Fig. 1f, Table 7).

Several important components of apatite exhibit strong correlations (Table 8); in addition to the excellent correlation shown between As and P (Fig. 7a), there are good correlations between As and Mn, as well as F (*cf.* Figs. 7b, c), and an excellent inverse correlation between Mn and P (Table 8). On the other hand, no correlation is observed between As and the minor constituents Sr and Fe. The correlated variations of As, P, Mn, and F probably result from the simultaneous operation of $As^{5+}P_{-1}$ and other, in principle independent exchange-vectors, *e.g.*, $(OH)F_{-1}$ and $MnCa_{-1}$. This result is similar to what has been observed for roméite and, again, suggests that the fluid composition may have exerted a control on these correlations. We should bear

in mind that although two generations of apatite may be distinguished in BSE images, both generations display the same chemical trends.

It is of note that at Starlera, we do not observe svabite, the As equivalent of fluorapatite, despite high As contents of the apatite. Svabite, $Ca_5(AsO_4)_3F$, is a characteristic mineral of some metamorphosed Mn deposits and occurs, for example, at Långban, Sweden (associated with bergslagite, Hansen *et al.* 1984), and at Franklin, New Jersey (Dunn 1995).

Bergslagite

The mineral bergslagite, $CaBeAsO_4(OH)$, has been discovered in the metamorphosed Mn ores of Långban, Sweden (Hansen *et al.* 1984). To date, bergslagite has been reported as a rare vug-filling mineral from three additional localities: in the radiolarite-hosted Mn ores at Falotta, Graubünden, Switzerland (Graeser 1995), in metarhyolites at Cavradi, Graubünden, Switzerland (Graeser 1995), and in rhyolites at Sailauf, Spessart, Germany (Kolitsch 1996). In Val Ferrera, bergslagite was observed as a rock-forming, post-D_1 mineral in the pink schists at Starlera, and in quartz–carbonate veins from a Be-, Mo-, W-, and Sb-rich pink dolomite breccia at Fianel (Brugger *et al.* 1998).

Bergslagite forms a solid solution with the phosphate mineral herderite, $CaBePO_4(F,OH)$ (Graeser 1995), but at both localities in Val Ferrera, the extent of the PAs^{5+}_{-1} substitution is very limited (≤0.45 wt% P_2O_5; Table 7). At Starlera, the composition of bergslagite is

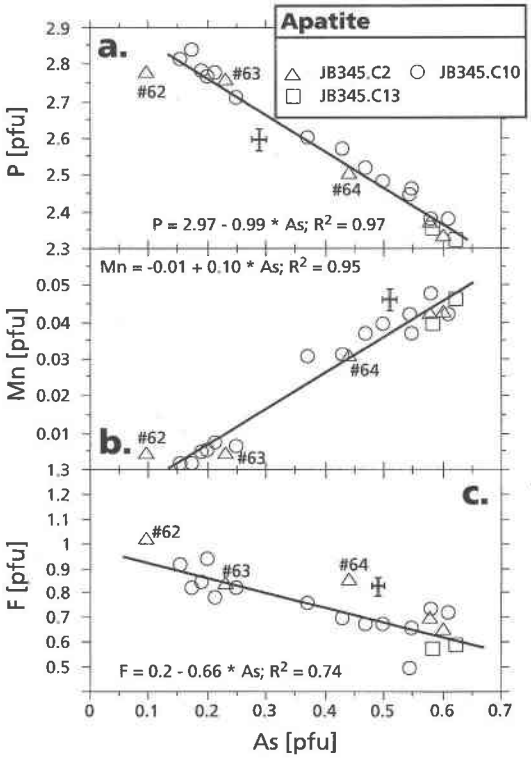

FIG. 7. Element correlations in fluorapatite from the pink schists at Starlera. The points corresponding to the compositions of the fluorapatite depicted in Figure 1f are labeled. Error bars correspond to 2σ and result from counting statistics.

TABLE 6. CORRELATION MATRIX FOR THE MAIN ELEMENTS PRESENT IN THE ROMEITE–BETAFITE FROM STARLERA

	Sb	Ti	Ca	Na	Mn	Ce
Ti	-0.99	1.00				
Ca	0.96	-0.96	1.00			
Na	0.96	-0.97	0.97	1.00		
Mn	-0.94	0.95	-0.97	-0.99	1.00	
Ce	-0.96	0.99	-0.96	-0.98	0.97	1.00
F	0.95	-0.96	0.98	0.98	-0.99	-0.96

Notes: n = 16; three data points (*cf.* Figs. 6c, d) have been omitted in these calculations; based on normalized electron-microprobe data.

TABLE 7. COMPOSITION OF FLUORAPATITE AND BERGSLAGITE, PINK SCHIST, STARLERA, SAMPLE JB345

	#62	#64	3	4	5
	Apatite			Bergslagite	
n	1	1	18	10	10
P_2O_5	39.06	34.19	30.92-39.54	0.32	0.24-0.45
As_2O_5	2.20	9.77	2.20-13.84	55.80	55.21-56.19
SiO_2	0.78	0.08	<0.01-0.78	0.18	0.06-0.38
Sb_2O_5	n.a.	n.a.	n.a.	0.04	<0.04-0.09
CaO	55.79	54.10	52.54-55.79	27.25	26.09-27.81
SrO	0.45	0.13	0.06-0.45	0.11	<0.03-0.20
Na_2O	<0.04	<0.04	<0.04	<0.04	<0.04
FeO	0.12	0.14	0.02-0.24	0.07	0.06-0.08
MnO	0.06	0.42	0.03-0.65	0.05	<0.05-0.07
Ce_2O_3	<0.03	<0.03	<0.03-0.08	0.11	<0.03-0.23
F	3.81	3.12	1.80-3.81	<0.05	<0.05
H_2O_{calc}		0.27	0-0.86		
-(F,Cl)	1.60	1.31			
Sum	100.70	100.89	99.10-103.51	83.94	81.93-84.84
Ca^{2+}	5.021	5.005	4.940-5.021	0.989	0.976-0.997
Sr^{2+}	0.022	0.007	0.003-0.022	0.002	0.004
Fe^{2+}	0.008	0.010	0.001-0.017	0.002	0.002
Mn^{3+}	0.004	0.031	0.002-0.048	0.001	0.002
Ce^{3+}				0.001	0.003
Σ(Ca sites)	*5.060*	*5.053*	*4.988-5.066*	*0.997*	*0.981-1.002*
P^{5+}	2.778	2.499	2.324-2.841	0.009	0.007-0.013
As^{5+}	0.097	0.441	0.097-0.623	0.988	0.983-1.008
Si^{4+}	0.066			0.006	0.002-0.013
Σ(P site)	*2.940*	*2.947*	*2.934-3.012*	*1.003*	*0.998-1.019*
F	1.012	0.852	0.50-1.01		
H^+		0.148	0.00-0.50		
Σ(Cl,F)	*1.012*	*1.000*			
O^{2-}	11.87	11.99	11.87-12.24		

Structural formulae are calculated on the basis of eight and two cations per formula unit for apatite and bergslagite, respectively. Electron-microprobe data, reported as weight %. n: number of points for average.
Column headings: 62: Core of crystal shown in Figure 1f. 64: Rim of crystal shown in Figure 1f. 3: Minimum and maximum values. 4: Mean value; addition of 1 OH and 1 Be per formula unit would raise the analytical total to 100.51%. 5: Minimum and maximum values.

TABLE 8. CORRELATION MATRIX FOR THE MAIN ELEMENTS IN THE APATITE FROM THE PINK SCHISTS AT STARLERA

	P	As	Ca	Mn
As	−0.98	1.00		
Ca	0.35	−0.49	1.00	
Mn	−0.97	0.98	−0.49	1.00
F	0.78	−0.84	0.61	−0.81

Notes: n = 21; based on the normalized results of electron-microprobe analyses.

further characterized by small amounts of Sb (<0.1 wt% Sb_2O_5), Si (≤0.38 wt% SiO_2), Sr (≤0.20 wt% SrO), Fe (≤0.08 wt% FeO), and Mn (≤0.07 wt% MnO). Neither F nor Na were detected, but Ce is present in concentrations up to 0.23 wt% Ce_2O_3.

Discussion

The mineral assemblage in the pink schists at Starlera is particularly interesting because several As, Sb, and Be minerals are present as rock-forming minerals. In contrast to other localities in Val Ferrera, however, these minerals do not occur in S_1 and, as suggested by petrographic observations, must have formed postkinematically with respect to the main deformational event (D_1). At least two stages of post-D_1 crystallization can be distinguished within the pink schists (Fig. 8). Moreover, the thick roméite–tilasite veins also formed after D_1; most are closely associated with the intensely foliated pink schists, suggesting that the foliation may have focused the flow of an As-, Sb-, and Ti-bearing fluid during vein formation. Relatively large amounts of fluid were required to generate these thick veins. The association of elements found in the post-D_1 assemblage of the pink schists and in the late roméite–tilasite veins are very similar (in particular As, Sb, and Ti), indicating that the post-D_1 assemblages in the schists were formed by the same fluid that generated the roméite–tilasite veins.

The elements that accumulated in the roméite–tilasite veins and in the post-D_1 minerals of the pink schists were probably derived from a local source, *e.g.*, the surrounding ores or the pink schists.

Titanium

Although Ti is an essential constituent of roméite in the late veins of Starlera, the carbonate-hosted Fe–Mn ores are Ti-poor (<0.10 wt% TiO_2, Brugger 1996). The pink schists, however, are fairly rich in Ti and are the only ore-related lithology where titanite and rutile have been identified. Microscopic observations indicate that Sb-poor rutile was present as a detrital mineral in the sedimentary protolith; furthermore, the micas contain considerable amounts of Ti (average 0.44 wt% TiO_2, Table 3). We therefore conclude that the pink schists are a possible source for the Ti concentrated in the roméite–tilasite veins.

Arsenic, antimony, and beryllium

The carbonate-hosted ores of Val Ferrera are characterized by elevated contents of As, Sb, and Be rela-

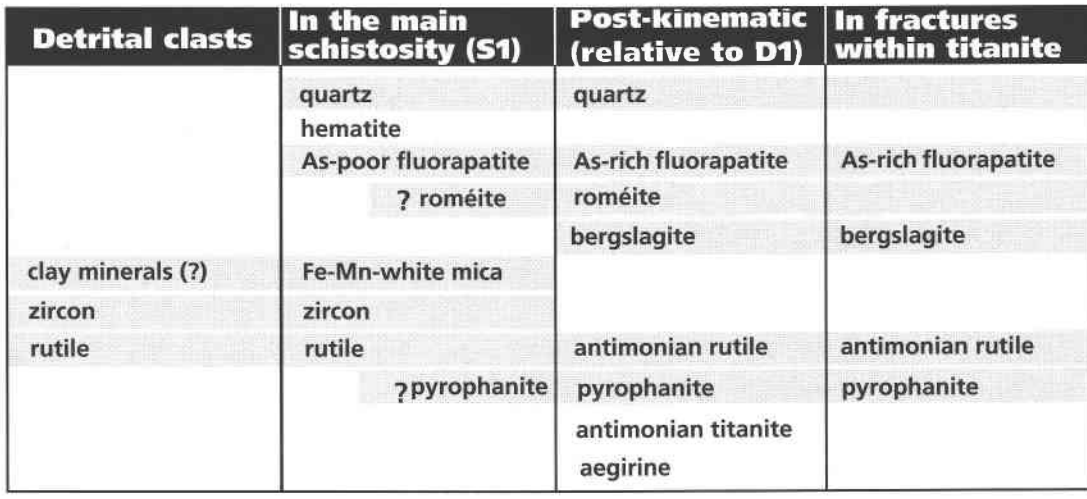

FIG. 8. Paragenetic evolution of the pink schists from Starlera. Postkinematic refers to deformational event D_1, which produced S_1.

tive to the country rocks (Brugger 1996). The growth in some deposits of As, Sb, and Be minerals during the main deformation (D_1) points to a pre-D_1 or, at the latest, syn-D_1 accumulation of these elements in the ores. At Starlera, concordant tilasite-rich lenses possibly represent the metamorphosed equivalent of As-rich hydrothermal sediments. Such high levels of As enrichments have not yet been reported from modern exhalative Mn deposits, although the latter commonly contain in excess of 100 ppm As (Marchig *et al.* 1982). On the other hand, several wt% As may be concentrated in other types of modern hydrothermal metalliferous sediments (*e.g.,* Karpov & Naboko 1990, Pearcy & Petersen 1990).

Thus, the large amounts of As, Sb, and Be concentrated in the post-D_1 assemblage of minerals in the pink schists and the discordant roméite–tilasite veins were most probably derived from the surrounding Fe–Mn ores. As outlined above, however, the pink schists lack syn-D_1 As, Sb, or Be minerals and, moreover, the white mica is poor in Sb (<200 ppm Sb). This finding may indicate that the unusual association of minerals in the pink schists is not related to anomalous concentrations of As, Sb, and Be in the protolith of the pink schists relative to the surrounding Fe–Mn ores, but to physical (permeability) and mineralogical (presence of detrital rutile) characteristics. Fluids enriched in As, Sb, and Be through interaction with the Fe–Mn ores were focused into the pink schists, where they became further enriched in Ti by reaction with mica and rutile.

A striking mineralogical characteristic of the pink schists at Starlera is the abundance of Sb in the three Ti minerals rutile, titanite, and pyrophanite. After Praborna, Starlera is only the second locality where Sb-rich varieties of rutile and titanite have been reported. Praborna is a small syngenetic-exhalative deposit interbedded within radiolarites that overlie mid-ocean ridge basalts of the Piemont nappe. This nappe was subjected to a Cretaceous eclogite-facies metamorphism, and subsequently underwent several episodes of retrograde metamorphism, terminating under greenschist-facies conditions in the early Tertiary (Martin-Vernizzi 1984). At Praborna, Sb-rich rutile and Sb-rich titanite developed during the greenschist-facies stage and were, at least in part, formed by metasomatic replacement of older Sb-free rutile and Sb-free titanite (Perseil 1991, Perseil & Smith 1995, Smith & Perseil 1997). The similarity in the history of Sb and Ti mobility at Starlera and Praborna, two deposits having different geological settings and overall patterns of metamorphic evolution, documents the local mobility of Ti and Sb in the lower greenschist facies and under relatively oxidizing conditions (above the magnetite–hematite buffer).

Another characteristic feature of the Starlera deposit is its elevated content of As and Be, in addition to Sb. Arsenic and Sb are geochemically similar semimetals, and thus, it is perhaps not surprising that the Sb-rich varieties of rutile and titanite host significant amounts of As (up to 0.54 and 3.46 wt% As_2O_5, respectively). To the best of our knowledge, Starlera is only the third locality where As- bearing titanite is reported. The first observation was made in the Binntal, Valais (Switzerland), where As-bearing titanite was found to crystallize in vugs with a unique suite of rare arsenites ($[As^{3+}O_3]^{3-}$); in this case, it was inferred that As substitutes for Ti as a trivalent cation (Krzemnicki & Gieré 1996, Krzemnicki 1996). At Starlera, however, As probably occurs as As^{5+} in both Ti and Si sites. As-bearing titanite also was reported from the Praborna Mn deposit (Perseil & Smith 1996).

Roméite is a widespread accessory mineral in several Fe–Mn deposits of Val Ferrera, but the specimens from the pink schists are unique because of their high Ce and Ti contents (up to 23.90 wt% Ce_2O_3; up to 23.00 wt% TiO_2). In contrast, the roméite crystals occurring in other Val Ferrera localities as well as those present in the roméite–tilasite veins at Starlera contain a maximum of only 4.22 wt% Ce_2O_3 and 8.26 wt% TiO_2 (Brugger *et al.* 1997). The composition of the roméite from the pink schists is intermediate between roméite $(Ca,Na,\square)_2Sb_2O_6(F,OH,O)$ and a hypothetical "ceriumbetafite-(Ce)" end-member $Ce_2Ti_2O_7$, similar to the existing end-member yttrobetafite-(Y), $(Y,U,Ce,\square)_2(Ti,Nb,Ta)_2O_6(OH,O)$ (Hogarth 1977). The composition of roméite in the pink schists illustrates the strong affinity of the pyrochlore structure for the *REE*, as all other minerals associated with roméite (including titanite and apatite) contain less than 0.3 wt% Ce_2O_3.

Acknowledgements

We thank Susanne Schmidt and Richard Guggenheim (EMP and SEM Laboratories, University of Basel) for providing access to their facilities. We are grateful to Daniel Mathys for supplying the BSE images, to Stefan Graeser, Michael Krzemnicki, and Peter Berlepsch for stimulating discussions, and to John F. Slack and David C. Smith for their thorough and helpful reviews. This work was funded through a grant from the Schweizerischer Nationalfonds (grant 2000–43350.95).

References

Abrecht, J. (1989): Manganiferous phyllosilicate assemblages: occurrences, composition and phase relations in metamorphosed Mn deposits. *Contrib. Mineral. Petrol.* **103**, 228-241.

Armbruster, T., Bühler, C., Graeser, S., Stalder, H.A. & Amthauer, G. (1988): Cervandonite-(Ce), $(Ce,Nd,La)(Fe^{3+},Fe^{2+},Ti^{4+},Al)_3SiAs(Si,As)O_{13}$, a new Alpine fissure mineral. *Schweiz. Mineral. Petrogr. Mitt.* **68**, 125-132.

Baudin, T. & Marquer, D. (1993): Métamorphisme et déformation dans la nappe de Tambo (Alpes centrales suisses): évolution de la substitution phengitique au cours de la déformation alpine. *Schweiz. Mineral. Petrogr. Mitt.* **73**, 285-299.

_____, _____, BARFETY, J.-C., KERCKHOVE, C. & PERSOZ, F. (1995): A new stratigraphical interpretation of the Mesozoic cover of the Tambo and Suretta nappes: evidence for early thin-skinned tectonics (Swiss Central Alps). *C.R. Acad. Sci., Paris* **321**, *sér.* **IIa**, 401-408.

BLACKBURN, W.H. & DENNEN, W.H. (1997): Encyclopedia of Mineral Names. *The Canadian Mineralogist, Spec. Publ.* **1**.

BONATTI, E. (1975): Metallogenesis at oceanic spreading centers. *Annu. Rev. Earth Planet. Sci.* **3**, 401-431.

BOSTRÖM, K., RYDELL, H. & JOENSUU, O. (1979): Långban – an exhalative sedimentary deposit? *Econ. Geol.* **74**, 1002-1011.

BOUCH, J., HOLE, M. & TREWIN, N. (1997): Rare earth and high field strength elements partitioning behaviour in diagenetically precipitated titanites. *Neues Jahrb. Mineral. Abh.* **172**, 3-21.

BRUGGER, J. (1996): *The Fe, Mn, (V, Sb, As, Be, W) deposits of Val Ferrera (Graubünden, Switzerland).* Ph.D. thesis, Institute for Mineralogy and Petrography, Basel, Switzerland.

_____ & BERLEPSCH, P. (1996): Description and crystal structure of fianelite $Mn_2V(V,As)O_7{\bullet}2H_2O$, a new mineral from Fianel, Val Ferrera, Graubünden, Switzerland. *Am. Mineral.* **81**, 1270-1276.

_____ & _____ (1997): Johninnesite $Na_2(Mn^{2+})_9(Mg,Mn)_7(AsO_4)_2(Si_6O_{17})_2(OH)_8$: a new occurrence in the Val Ferrera (Graubünden, Switzerland). *Schweiz. Mineral. Petrogr. Mitt.* **77**, 449- 455.

_____, GIERÉ, R., GRAESER, S. & MEISSER, N. (1997): The crystal chemistry of roméite. *Contrib. Mineral. Petrol.* **127**, 136-146.

_____, _____, GROBETY, B. & USPENSKY, E. (1998): Scheelite–powellite and paraniite-(Y) from the Fe–Mn deposit at Fianel, eastern Swiss Alps. *Am. Mineral.* **83**, 1100-1110.

ČERNÝ, P., ČECH, F. & POVONDRA, P. (1964): Review of ilmenorutile–strüverite minerals. *Neues Jahrb. Mineral., Abh.* **101**, 142-172.

CHOPIN, C. (1978): Les paragenèses réduites ou oxydées des concentrations manganèsifères des "schistes lustrés" de Haute-Maurienne (Alpes françaises). *Bull. Minéral.* **101**, 514-531.

CORTESOGNO, L., LUCCHETTI, G. & PENCO, A.M. (1979): Le mineralizzazioni a manganese nei diaspri delle ofioliti liguri: mineralogia e genesi. *Rend. Soc. Ital. Mineral. Petrol.* **35**, 151-197.

DAMOUR, A. (1841): Sur la roméite, nouvelle espèce minérale, de St. Marcel, Piemont. *Ann. Minéral.* **20**(3), 247.

DASGUPTA, S., SENGUPTA, P., BHATTACHARYA, P.K., MUKHERJEE, M., FUKUOKA, M., BANERJEE, H. & ROY, S. (1989): Mineral reactions in manganese oxide rocks: P–T–X phase relations. *Econ. Geol.* **84**, 434-443.

DEER, W.A., HOWIE, R.A. & ZUSSMAN, J. (1982): *Rock-Forming Minerals.* **1A**. *Orthosilicates.* Longman, London, U.K.

DUNN, P.J. (1991): Rare minerals of the Kombat mine, Namibia. *Mineral. Rec.* **22**, 421-424.

_____ (1995): *Franklin and Sterling Hill, New Jersey: the World's Most Magnificent Mineral Deposits.* Privately published, Franklin, N.J.

FOORD, E.E., HLAVA, P.F., FITZPATRICK, J.J., ERD, R.C. & HINTON, R.W. (1991): Maxwellite and squawcreekite, two new minerals from the Black Range tin district, Catron County, New Mexico, USA. *Neues Jahrb. Mineral., Monatsh.*, 363-384.

GAKIEL, U. & MALAMUD, M. (1969): On the valence of iron in tripuhyite: a Mössbauer study. *Am. Mineral.* **54**, 299-301.

GEIGER, T. (1948): Manganerze in den Radiolariten Graubündens. *Beiträge zur Geologie der Schweiz, Geotechnische Ser.* **27**.

GIERÉ, R. (1992): Compositional variation of metasomatic titanite from Adamello (Italy). *Schweiz. Mineral. Petrogr. Mitt.* **72**, 167-177.

GRAESER, S. (1995): Bergslagit aus den Schweizer Alpen. *Aufschluss* **46**, 15-22.

HANSEN, S., FÄLTH, L., PETERSEN, O.V. & JOHNSEN, O. (1984): Bergslagite, a new mineral species from Långban, Sweden. *Neues Jahrbuch Mineral., Monatsh.*, 257-262.

HAYWARD, P.J. (1988): Glass-ceramics. *In* Radioactive Waste Forms for the Future (W. Lutze & R.C. Ewing, eds.). North Holland, Amsterdam, The Netherlands (427-494).

HOGARTH, D.D. (1977): Classification and nomenclature of the pyrochlore group. *Am. Mineral.* **62**, 403-410.

HOLTSTAM, D., NYSTEN, P. & GATEDAL, K. (1998): Parageneses and compositional variations of Sb oxyminerals from Långban-type deposits in Varmland, Sweden. *Mineral. Mag.* **62**, 395-407.

HURFORD, A.J., FLYSCH, M. & JÄGER, E. (1989): Unraveling the thermo-tectonic evolution of the Alps: a contribution from fission track analysis and mica dating. *In* Alpine Tectonics (M.P. Coward, D. Dietrich & R.G. Park, eds.). *Geol. Soc., Spec. Publ.* **45**, 369-398.

HUSSAK, E. & PRIOR, G.T. (1897): On tripuhyite, a new antimonate of iron, from Tripuhy, Brazil. *Mineral. Mag.* **11**, 302-303.

KARPOV, G.A. & NABOKO, S.I. (1990): Metal contents of recent thermal waters, mineral precipitates and hydrothermal alteration in active geothermal fields, Kamchatka. *J. Geochem. Explor.* **36**, 57-71.

KOLITSCH, U. (1996): Bergslagit aus dem Rhyolitstreinbruch bei Sailauf, Spessart. *Mineralien Welt* **7**, 45-46.

KRZEMNICKI, M.S. (1996): *Mineralogical Investigations on Hydrothermal As- and REE-Bearing Minerals within the Gneisses of the Monte Leone Nappe (Binntal Region, Switzerland).* Ph.D. thesis, University of Basel, Basel, Switzerland.

_____ & GIERÉ, R. (1996): As-REE-bearing titanite from the Monte Leone nappe (Binntal, Switzerland). *Schweiz. Mineral. Petrogr. Mitt.* **76**, 117-118.

KUNZ, M., XIROUCHAKIS, D., WANG, Y.B., PARISE, J.B. & LINDSLEY, D.H. (1997): Structural investigations along the join $CaTiOSiO_4$ – $CaSnOSiO_4$. *Schweiz. Mineral. Petrogr. Mitt.* **77**, 1-11.

LINIGER, M. (1992): *Der ostalpin-penninische Grenzbereich im Gebiet der nördlichen Margna- Decke (Graubünden, Schweiz).* Ph.D. thesis, ETH, Zürich, Switzerland.

MARCHIG, V., GUNDLACH, H., MÖLLER, P. & SCHLEY, F. (1982): Some geochemical indicators for discrimination between diagenetic and hydrothermal metalliferous sediments. *Marine Geol.* **50**, 241- 256.

MARTIN-VERNIZZI, S. (1984): *La mine de Praborna (Val d'Aoste, Italie) : une série manganèsifère métamorphisée dans le faciès éclogite.* Thèse de doctorat, Univ. Pierre et Marie Curie, Paris, France.

MASON, B. & VITALIANO, C. J. (1953): The mineralogy of the antimony oxides and antimonates. *Mineral. Mag.* **30**, 100-112.

MASSONNE, H.J. & SCHREYER, W. (1987): Phengite geobarometry based on the limiting assemblage with K-feldspar, phlogopite, and quartz. *Contrib. Mineral. Petrol.* **96**, 212-224.

MOORE, P.B. (1968): Substitutions of the type $(Sb^{5+}_{0.5}Fe^{3+}_{0.5}) = (Ti^{4+})$: the crystal structure of melanostibite. *Am. Mineral.* **53**, 1104-1109.

MOTTANA, A. & GRIFFIN, W.L. (1979): Pink titanite (greenovite) from St Marcel, Valle d'Aosta, Italy. *Rend. Soc. Ital. Mineral. Petrol.* **35**, 135-143.

PAN, YUANMING & FLEET, M.E. (1992): Mineral chemistry and geochemistry of vanadian silicates in the Hemlo gold deposit, Ontario, Canada. *Contrib. Mineral. Petrol.* **109**, 511-525.

PATERSON, B.A. & STEPHENS, W.E. (1992): Kinetically induced compositional zoning in titanite: implications for accessory-phase/melt partitioning of trace elements. *Contrib. Mineral. Petrol.* **109**, 373-385.

PEARCY, E.C. & PETERSEN, U. (1990): Mineralogy, geochemistry and alteration of the Cherry Hill, California hot-spring gold deposit. *J. Geochem. Explor.* **36**, 143-169.

PERSEIL, E.-A. (1991): La présence du Sb-rutile dans les concentrations manganésifères de St. Marcel – Praborna (Val d'Aoste – Italie). *Schweiz. Mineral. Petrogr. Mitt.* **71**, 341-347.

_____ & SMITH, D.C. (1995): Sb-rich titanite in the manganese concentrations at St. Marcel – Praborna, Aosta Valley, Italy: petrography and crystal-chemistry. *Mineral. Mag.* **59**, 717-734.

_____ & _____ (1996): Cristallochimie de l'arsenic dans la fluorapatite et la titanite des concentrations manganésifères de St. Marcel – Praborna, V. Aoste (Italie). *Abstr., 16ème Réunion des Sciences de la Terre (Orléans)*, 167.

PETERS, T., TROMMSDORFF, V. & SOMMERAUER, J. (1980): Progressive metamorphism of manganese carbonate and cherts in the Alps. *In* Geology and Geochemistry of Manganese (I.M. Varentsov & G. Grassely, eds.). Schweizerbart'sche Verlagsbuchhandlung, Stuttgart, Germany (271-283).

ROY, S. (1968): Mineralogy of the different genetic types of manganese deposits. *Econ. Geol.* **63**, 760-786.

RUSSELL, J.K., GROAT, L.A. & HALLERAN, A.A.D. (1994): *LREE*-rich niobian titanite from Mount Bisson, British Columbia: chemistry and exchange mechanisms. *Can. Mineral.* **32**, 575-587.

SCHMID, S.M., PFIFFNER, O.A. & SCHREURS, G. (1997): Rifting and collision in the Penninic zone of eastern Switzerland. *In* Deep Structure of the Swiss Alps – Results from NFP/PNR 20 (A. Pfiffner, ed.). Birkhäuser AG, Basel, Switzerland (160-185).

SHANNON, R.D. (1976): Revised effective ionic radii and systematic studies of interatomic distances in halides and chalcogenides. *Acta Crystallogr.* **A32**, 751-767.

SMITH, D.C. & PERSEIL, E.-A. (1997): Sb-rich rutile in the manganese concentrations at St. Marcel – Praborna, Aosta Valley, Italy: petrology and crystal-chemistry. *Mineral. Mag.* **61**, 655-669.

STORMER, J.C., JR., PIERSON, M.L. & TACKER, R.C. (1993): Variation of F and Cl X-ray intensity due to anisotropic diffusion in apatite during electron microprobe analysis. *Am. Mineral.* **78**, 641-648.

STUCKY, K. (1960): Die Eisen- und Manganerze in der Trias des Val Ferrera. *Beiträge zur Geologie der Schweiz, Geotechnische Ser.* **37**.

TRÜMPY, R. (1980): *Geology of Switzerland, a Guide Book. A. An Outline of the Geology of Switzerland.* Schweizerische geologische Kommission, Wepf, Basel, Switzerland.

VON BLANCKENBURG, F. (1992): Combined high-precision chronometry and geochemical tracing using accessory minerals: applied to the Central-Alpine Bergell intrusion (central Europe). *Chem. Geol.* **100**, 19-40.

Received April 7, 1997, revised manuscript accepted December 28, 1998.